PERGAMON

International Journal of Heat and Mass Transfer 41 (1998) 3919–3935

International Journal of HEAT and MASS TRANSFER

Classification of one-dimensional steady-state two-phase geothermal flows including permeability variations—I. Theory and special cases

R. M. Young*

N.Z. Institute for Industrial Research and Development, P.O. Box 31-310, Lower Hutt, New Zealand

Received 24 July 1996; in final form 12 February 1998

Abstract

This paper describes a graphical method for classifying reservoir models of the above type, and for clarifying the connection between permeability (and permeability gradients) and saturation. The theory behind the method is reviewed, and then the technique is applied to the example of a bottom-heated geothermal heatpipe, which is shown to have a maximum length, beyond which the only possible stable continuation (downwards) is into single-phase vapour. A permeability increase (downwards) always acts to induce a liquid saturation increase. A similar conclusion holds for non-zero net mass flow but with no conduction. Our theoretical results agree with those obtained by numerical simulation.

1. Introduction

The role played by permeability in single-phase porous media flow is well understood, at least in principle. In steady-state flow, for example, it follows from Darcy's law that low permeabilities should give rise to high pressure gradients and large pressure changes. However, the corresponding situation for two-phase (steam/water) porous media flow is more complicated. The absolute permeability in Darcy's law is now multiplied by a function of saturation (the relative permeability), which implies that saturation as well as pressure gradient will be strongly influenced by the permeability distribution.

Previous work. Low permeability barriers (e.g. caprock formations) have been associated with the formation of vapour-dominated geothermal reservoirs. Schubert and Straus [1] examined the gravitational stability of water over steam and concluded that this was only possible for low permeabilities ($k < 4 \times 10^{-17}\,\mathrm{m}^2$). Since most vapour-dominated systems have reservoir permeabilities at least two orders of magnitude greater than this they concluded (Straus and Schubert [2]) that a permeability contrast was required for the development of such a system in the natural state. The phase boundary between the single-phase groundwater zone and the two-phase vapour-dominated reservoir would then occur in the low permeability caprock; below this there would be a rapid transition to high permeability reservoir conditions (still vapour-dominated).

The work of Schubert and Straus was based on a consideration of the one-dimensional steady-state, and the integration of the steady-state equations. Ingebritsen and Sorey [3] carried out two-dimensional numerical simulations of a reservoir bounded by a low permeability 'aureole' (consisting of a caprock, and low permeability lateral boundaries). They found in their examples that vapour-dominated conditions evolved in the reservoir provided the caprock permeability was sufficiently small ($k < 10^{-16}\,\mathrm{m}^2$) and reservoir permeability was sufficiently large ($k > 10^{-15}\,\mathrm{m}^2$).

Stubos et al. [4] have made a theoretical investigation of the effects of permeability heterogeneity. Their work involves explicit consideration of capillary effects, but neglects conduction. The results are given for a one-dimensional steady-state heatpipe. Stubos et al. find that if the heatpipe is liquid-dominated, then a positive permeability discontinuity (k increasing downward) acts to

* Corresponding author. Tel.: 0064 4 5690247; fax: 0064 4 5690003; e-mail: roger@maths.grace.cri.nz

0017–9310/98 $19.00
PII: S0017–9310(98)00089–1

decrease the liquid saturation. This would seem to support Schubert and Straus' hypothesis that vapour-dominated conditions could be associated with a permeability increase. However Stubos et al. also state that if the permeability variation is sufficiently weak then precisely the opposite happens, that is, a positive permeability gradient (k increasing downward) acts to increase (rather than decrease) the liquid saturation.

Method and aims of this paper. The studies just mentioned all give partial results, based either on a numerical analysis of particular cases (Ingebritsen and Sorey), or on a restricted set of physical parameters (Stubos et al.). In this paper we shall remove some of these restrictions, and examine the interrelation of permeability, saturation and pressure in a wider context. Nevertheless we will still require that the flows fulfil certain conditions, discussed in detail below. The main restriction is that the flows are required to be one-dimensional and steady-state, which has as a consequence that the mass and energy fluxes (J_M, J_E) are spatially constant. The complete set of one-dimensional steady-state geothermal flows can then be characterized as trajectories in a six-dimensional space whose degrees of freedom are mass flux (J_M), energy flux (J_E), permeability (k), thermal conductivity (K), pressure (P), and temperature (T) or liquid saturation (S) in the single-phase and two-phase regions, respectively. The geometry of this space is rather complicated. However it is neither necessary nor appropriate at this stage to go into the mathematical details (which are, however, purely algebraic—no differential equations need be solved). It turns out that all the important features of the two-phase part of the parameter space can be represented graphically in terms of certain two-dimensional diagrams labelled by a given (J_M, J_E, K), in which only permeability (k), pressure (P), and saturation (S) vary. The method is thus especially relevant to the study of the natural state of actual geothermal fields which can be modelled (approximately) as one-dimensional steady-state flows with known J_M, J_E and K.

In this paper we use special coordinates (w, s) defined in terms of the five field parameters (J_M, J_E, k, K, P) to parametrize the two-dimensional subspace, referred to here as the flowplane (see [5]). Pressure trajectories and contours are represented by one-parameter families of curves in the flowplane, and the saturation associated with each flowpoint is determined by a simple geometrical construction.

The systematic use of the flowplane diagram permits a complete classification of all possible one-dimensional steady-state geothermal flows. Qualitatively different phenomena are observed when the mass and energy flows exceed a well-defined watershed, likewise when the permeability is varied through certain critical values. Given the permeability profile, the flowplane diagram permits the construction of the state trajectory, which represents the state of the reservoir at any depth, in particular whether it is single-phase/two-phase, liquid-dominated/vapour-dominated, etc. The terminal state of the reservoir at depth may also be predicted.

In Part 1 of this paper we describe the methodology, and also consider in detail some special cases: (a) the case of zero net mass flux; and (b) the case of no conduction. Our treatment of these examples is compared with the results obtained by other authors including those cited above.

The main reason for the analysis of these special cases is, however, as a preparation for Part 2 of this paper where the general situation is considered, without restrictions on conduction and mass flow. We shall show that each of these effects has its own special geometrical signature in the flowplane which we identify separately in Part 1: however, taken together, they possess an important additional feature which we will discuss in Part 2.

Model assumptions. We confine our attention to porous media models which satisfy the following criteria:

(1) Models are restricted to be one-dimensional and steady-state. In the geothermal context the natural state is often assumed to be one of steady flow, or close to it. The assumption that the flow is one-dimensional (vertical) is legitimate for laboratory experiments, but is more problematic for geothermal reservoirs, where the central upflow is usually surrounded by steady-state convection cells. Nevertheless it is common practice to begin with a one-dimensional numerical model of an unexploited reservoir, the justification being that it has fewer unknown parameters, is more easily integrated, etc. Also if the one-dimensional model can be regarded as an approximation to a three-dimensional model, or as representing the central upflow of the latter, then it can help with the interpretation of the larger model. We believe that the phenomena which are characteristic of one-dimensional flow must also be present in some sense in a multidimensional model. Other phenomena may appear with increasing dimensionality, but it is important to have a good understanding of the basic (one-dimensional) case so that these multidimensional effects can be reliably identified.

(2) It is assumed that a two-phase zone exists somewhere at depth. Attention is restricted to boundary conditions which are physically realistic for geothermal reservoirs in the natural state. By this is meant that the model must be extendible upwards to the surface where a 1 bar pressure boundary condition, and a suitable temperature boundary condition, are applied. Mass and energy flows which originate with the geothermal source at depth are spatially constant, as follows from Assumption 1. We refer to these as BH-BC: bottom-heated boundary conditions. Under these conditions it can be shown that the saturation wave-speed [5] in the two-phase region is negative (points vertically upward). Furthermore, we may require an acceptable model to be extendible downward until single-phase or super-critical conditions are encountered.

(3) The relative permeability factors k_α for liquid ($\alpha = w$) and vapour ($\alpha = s$) are taken to be monotonic increasing (resp. decreasing) functions of liquid saturation, and there are residual saturations S_{rw} (S_{rs}) for which the liquid (resp. vapour) phase is immobile. In this paper we make the simplifying assumption [6, 2, 7] that the relative permeabilities add to unity

$$k_w + k_s = 1. \tag{1}$$

This restriction is not universally accepted. In particular Piquemal [8[has shown experimentally that for unconsolidated porous media $k_w + k_s \ll 1$. However we believe that the methods outlined in this paper will continue to be applicable in the more general case when (1) is relaxed. McGuinness [9] has noted the general insensitivity of the solution trajectories in the temperature–saturation phase plane to the choice of the relative permeability functions:

(4) Capillarity is not explicitly included in our formulation. Nevertheless the macroscopic effects of capillarity which have been noted by other authors [10] are actually implicit in the flowplane diagram (Fig. 1) on which our analysis is based. Young [5] has shown that the effects of a short range diffusive mechanism such as capillarity can be represented in the flowplane in terms of rules governing the sign of the saturation wavespeed (relative to the boundary conditions) and the types of phase transition which may occur. In particular the selection rules [4] which govern the choice of the correct saturation branch for the BH-BC described above are fully-accounted for in the flowplane diagram.

In addition, in this paper we limit the variations of absolute permeability and conductivity as follows: (1) As regards permeability we shall concentrate on permeability discontinuities, which are idealizations of rapid permeability contrasts. In a more general formulation permeability would be allowed to vary arbitrarily with depth. (2) Conductivity is taken to be constant with depth, which is probably a reasonable approximation provided there are no low-conductivity (insulating) layers within the medium.

Stability. The selection rules referred to above can also be related to the stability of the steady-state system. If the 'wrong' saturation branch is selected (relative to the imposed boundary conditions) then it remains a legitimate solution of the geothermal steady-state equations. However it cannot be obtained as the long time limit of a solution to the dynamic equations, and hence is not a steady-state solution in that sense. If this pseudo steady-state is taken as the initial state for a time-dependent geothermal simulation then it will quickly prove to unstable. This is the stability concept which is implicit in our work. It is based ultimately on the physical phenomenon of capillarity, and hence can be referred to as capillary stability. As mentioned above, Schubert and Straus [1] employ another concept, that of gravitational stability, in discussing their models. This refers to the stability of the one-dimensional system when subject to perturbations in two or three dimensions. They develop stability criteria based on permeability for their models. Capillary stability, on the other hand, can be formulated in a purely one-dimensional context, and is independent of permeability. We shall not consider gravitational stability further in this paper.

Plan of this paper. In the first section we summarize the geothermal equations used in this paper. In the next section we introduce the flowplane diagram following the presentation given in [5], and then explain the practical details of its construction and interpretation. This is followed by two sections which give the details of the diagram in the two cases already mentioned.

Conventions used in this paper. Depth (z) is positive vertically downwards. In the diagrams pressure is measured in bars (1 bar = 10^5 Pa) and permeability is measured in millidarcies (1 millidarcy = 1 md = 10^{-3} darcy = 10^{-15} m^2). We use the term saturation to mean liquid saturation when not otherwise specified, and often use saturation as a synonym for liquid relative permeability.

2. The geothermal equations

The geothermal equations are well-known in the literature, see for example [7]. They are derived from the standard conservation equations for mass and energy flow

$$\frac{\partial M}{\partial t} + \nabla \cdot \mathbf{J}_M = 0 = \frac{\partial E}{\partial t} + \nabla \cdot \mathbf{J}_E. \tag{2}$$

The mass and energy densities M, E are given as functions of the primary dependent variables which are usually taken to be pressure P and temperature T in single-phase conditions, while in two-phase conditions it is convenient to take pressure P and liquid saturation S as the principal variables. In the case of one dimension, and in the steady-state, the conservation equations reduce to the requirement that the fluxes of mass and energy are spatially constant:

$$J_M = \text{const}, \quad J_E = \text{const}. \tag{3}$$

In single-phase conditions these fluxes are

$$J_M = J_\alpha, \quad J_E = h_\alpha J_\alpha - K\frac{\mathrm{d}T}{\mathrm{d}z} \tag{4}$$

where J_α, $\alpha = w, s$ is the mass flow of liquid (w) or vapour (s), h is the enthalpy of the relevant phase, and K is the conductivity. The Darcy flows J_α in one dimension (vertical) are

$$J_\alpha = -\frac{k}{v_\alpha}\left(\frac{\mathrm{d}P}{\mathrm{d}z} - \rho_\alpha g\right) \tag{5}$$

where k is the absolute permeability (a function of depth), g is the acceleration due to gravity (z-axis positive down-

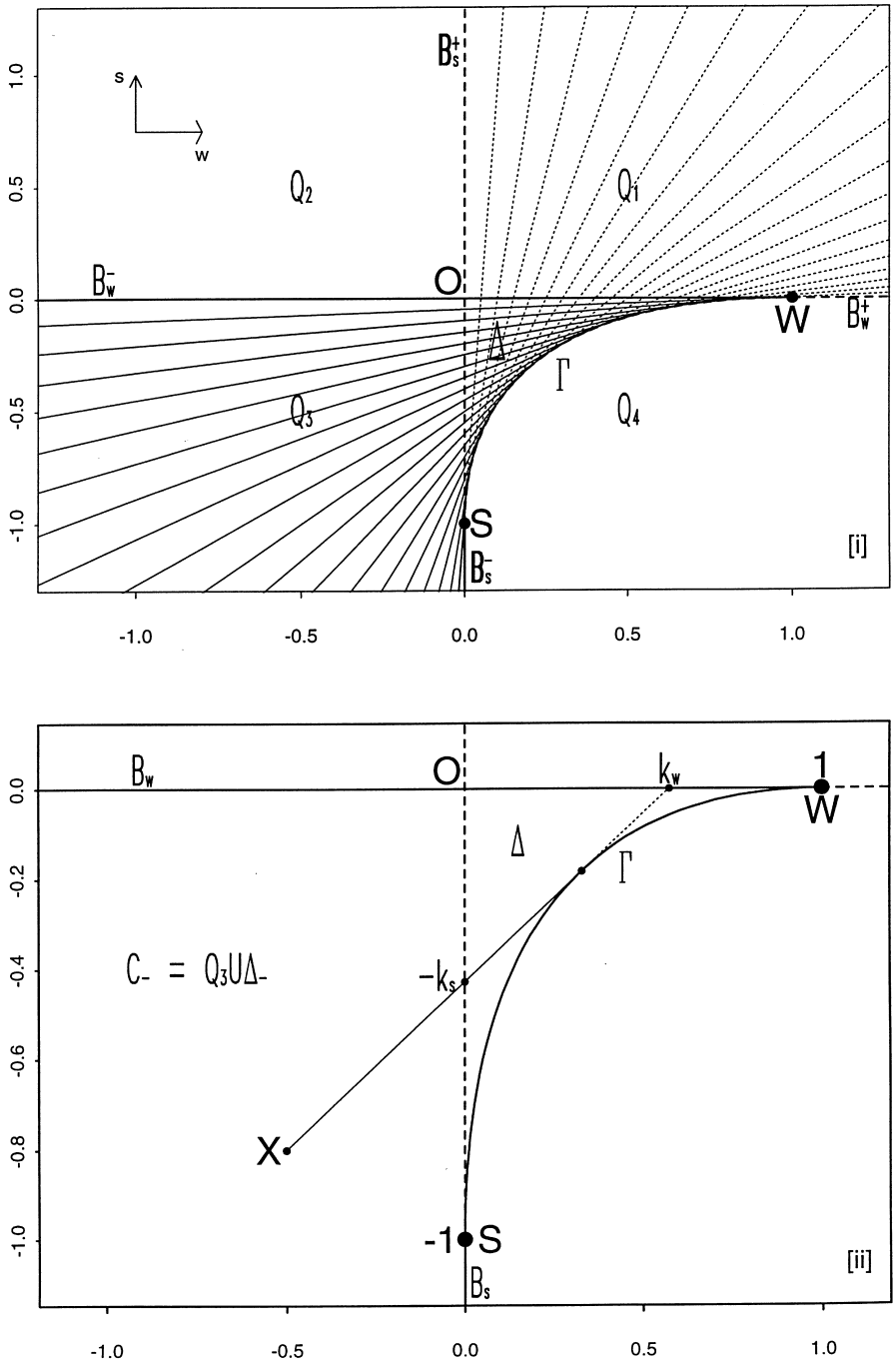

Fig. 1. The flowplane with coordinates (w, s), see equation (9) defined as the union of all the saturation lines (11). In [i] the solid lines fill out the region $Q_3 \bigcup \Delta$, where Q_3 is the third quadrant, and Δ is the part of the fourth quadrant defined by the saturation line envelope Γ which is tangent to the axes at the 'wet point' W(1, 0) and 'dry point' S(0, -1), respectively. Similarly the dotted lines pick out the region $Q_1 \bigcup \Delta$ where Q_1 is the first quadrant of the flowplane. The boundary segments are B_w^- : $(s = 0;\ -\infty < w < 1)$, B_w^+ : $(s = 0; 1 < w < \infty$, B_s^- : $(w = 0;\ -\infty < s < -1)$ and B_s^+ : $(w = 0; -1 < s < \infty)$. In [ii] we show the lower sheet $C_- = Q_3 \bigcup \Delta_-$ of the flowplane, origin O. The boundary of C_- is the union of the liquid boundary B_w $(s = 0; -\infty < w < 1)$, the vapour boundary B_s $(w = 0; -\infty < s < -1)$, and Γ. The saturation at the flowpoint X(w, s) is determined graphically by drawing the right tangent through X to Γ; the intercepts of the tangent on the axes give the relative permeabilities k_w, $-k_s$.

wards), and ρ_α, v_α are the density and kinematic viscosity of the relevant phase.

In two-phase conditions there are separate liquid and vapour fluxes so that

$$J_M = J_w + J_s \tag{6a}$$

$$J_E = h_w J_w + h_s J_s - K\frac{\mathrm{d}T_{\mathrm{sat}}}{\mathrm{d}z} \tag{6b}$$

where $T_{\mathrm{sat}}(P)$ is the saturation temperature, and the Darcy flows J_α, $\alpha = w, s$, are similar to (5) except for the introduction of relative permeability factors $k_\alpha(S)$

$$J_\alpha = -\frac{kk_\alpha}{v_\alpha}\left(\frac{\mathrm{d}P}{\mathrm{d}z} - \rho_\alpha g\right). \tag{7}$$

A useful relationship between pressure and saturation may be obtained by eliminating the pressure gradient between equations (6) and (7). It may be written in the form

$$\frac{s(P)}{k_s(S)} - \frac{w(P)}{k_w(S)} = -1 + i(P)\frac{1-k_w-k_s}{k_w k_s}. \tag{8}$$

In (8) the dimensionless coefficient functions w, s, i are functions of pressure (P), and also of the mass and energy flows (J_E, J_M), permeability (k) and conductivity (K)

$$w = \frac{-v_w}{g\Delta h\Delta\rho}\left[\left(\frac{J_E}{k}\right) - h_s\left(\frac{J_M}{k}\right) + \rho_s g\left(\frac{K}{k}\right)\frac{\mathrm{d}T_{\mathrm{sat}}}{\mathrm{d}P}\right] + i \tag{9a}$$

$$s = \frac{v_s}{g\Delta h\Delta\rho}\left[\left(\frac{J_E}{k}\right) - h_w\left(\frac{J_M}{k}\right) + \rho_w g\left(\frac{K}{k}\right)\frac{\mathrm{d}T_{\mathrm{sat}}}{\mathrm{d}P}\right] - i \tag{9b}$$

$$i = \frac{v_w v_s}{g\Delta h\Delta\rho}\left(\frac{J_M}{k}\right)\left(\frac{K}{k}\right)\frac{\mathrm{d}T_{\mathrm{sat}}}{\mathrm{d}P} \tag{9c}$$

where $\Delta h = h_s - h_w$, $\Delta\rho = \rho_w - \rho_s$. Note that the second term on the right of equation (8) is zero when either (a) conductivity K is zero; or (b) net mass flow J_M is zero (a heatpipe); or (c) the normalization (1) applies. For future reference note also that when either (a) or (b) holds the ratio w/s is independent of permeability.

Field equations for the primary variables may be derived from the conservation equations (2). The pressure equation is parabolic in character, and in single-phase conditions so is the temperature equation (assuming some conduction). However in two-phase conditions (and excluding capillarity) the saturation equation is hyperbolic

$$\frac{\partial S}{\partial t} + \mathbf{C}\cdot\nabla S = \delta - \beta\cdot\nabla k \tag{10}$$

where the saturation wavespeed vector $\mathbf{C}$ has the functional form $\mathbf{C} = \mathbf{C}(\nabla P, P, S, k)$ and the forcing function δ depends on these variables, and on P_t as well. The second term on the right is a source term resulting from the permeability heterogeneity, and the coefficient β has the functional form $\beta = \beta(S, P, k)$. We shall not require specific expressions for C, δ and β in this paper (see [11] and [12]).

3. The flowplane diagram

In some recent papers Young [12, 5] has employed flowplane coordinates w, s to represent the geothermal two-phase state. These coordinates are linearly related to the mass and energy flows through the defining equations (9). Assuming the normalization (1), equation (8) implies that a given saturation $S = \text{const}$ is represented by a straight line in the flowplane

$$\frac{w}{x} - \frac{s}{1-x} = 1 \tag{11}$$

where $x \equiv k_w(S) = 1 - k_s$. As x varies from 0–1 the saturation lines fill out a certain region in the flowplane and thus define the complete set of possible two-phase states as indicated in Fig. 1(i). The curve Γ in this figure is the envelope of the saturation lines (11). A simple calculation shows that Γ is a parabolic arc

$$\sqrt{w} + \sqrt{-s} = 1 \tag{12}$$

which touches the w-axis at the 'wet point' W(1, 0) and the s-axis at the 'dry point' S(0, −1). The two-phase region of the flowplane is then manifestly $\mathrm{C} = \mathrm{Q}_1 \bigcup \mathrm{Q}_3 \bigcup \Delta$ where Q_1, Q_3 are the first and third flowplane quadrants, and Δ is the part of the fourth quadrant Q_4 bounded by the flowplane axis and Γ.

Alternatively we may write (11) as a quadratic in x

$$x^2 - x(1 + w + s) + w = 0. \tag{13}$$

Then given a point $\mathrm{X}(w, s)$ in the flowplane, the associated saturation (or, more precisely the relative permeability) is determined by drawing the tangent to Γ through X as shown in Fig. 1(ii) [5]. The intercept of this line on the w-axis is the value of k_w, the intercept on the s-axis is $-k_s$. If X lies in Δ then there are two such tangents corresponding to the two roots of the quadratic (13). We use the notation $\Delta_-(\Delta_+)$ to indicate that the right (left) tangent should be chosen to specify the saturation branch.

It may be established [12] that the saturation wavespeed C is zero along Γ, and that $C \leqslant 0$ everywhere on the negative sheet $\mathrm{C}_- \equiv \mathrm{Q}_3 \bigcup \Delta_-$ of the flowplane. The corresponding positive sheet $\mathrm{C}_+ \equiv \mathrm{Q}_1 \bigcup \Delta_+$ has $C \geqslant 0$ everywhere. The positive (C_+) and negative (C_-) sheets are joined along Γ. It is shown in [5] that states for which $C > 0$ are unstable relative to BH-BC whereas those for which $C < 0$ are stable. Thus, C_+ is the unstable sheet of the flowplane and C_- is the stable sheet (relative to BH-BC), and $\Gamma = \mathrm{C}_+ \bigcap \mathrm{C}_-$ is the stability boundary. Consequently the two-phase states considered in this paper are restricted to lie on the negative sheet of the flowplane C_-.

Figure 1 is a universal diagram, that is, the construction is expressed solely in terms of the flowplane coordinates, and is valid for all relative permeability functions satisfying (1). This is the primary reason for introducing the complicated transformation (9).

The flowplane coordinates depend linearly on the mass and energy flows and on conductivity, but they are also non-linear functions of permeability and pressure (through the thermodynamic functions). Thus the flowplane diagram can be used in various ways, for example (a) to represent the totality of flowstates J_E, J_M (for constant k, K, P) see [12]; (b) to represent a parametrized set of pressure trajectories $w(P)$, $s(P)$ for each k but constant (J_M, J_E, K); or, (c) to represent a parametrized set of pressure contours $w(k)$, $s(k)$ for each P but constant (J_M, J_E, K). The representations (b) and (c) are used in this paper and are particularly suitable for characterizing the natural state of a given geothermal field which can be idealized as a one-dimensional upflow with known J_E, J_M, but with vertically varying permeability and pressure.

For such a field the permeability and pressure distribution with depth are probably not available, especially in the unexploited state. If the upflow contains a two-phase region the flowplane method can be used to examine the totality of permeability and pressure distributions which are compatible with the given mass and energy flows. While this might seem like an impossibly vague task, in fact in many situations there are severe constraints on the character of the flows.

3.1. Pressure trajectories and contours in the flowplane: a method

We will now explain the methodology for constructing and interpreting the flowplane diagram. We proceed by developing a series of representative examples. The representative Fig. 2 shows solid-line pressure trajectories (labelled by permeabilities measured in millidarcies) and dotted-line pressure contours (labelled by pressures measured in bars). This figure and those that follow have been constructed from the parametric representation (9) with J_M, J_E and K held constant. Fig. 2(i) illustrates a non-conductive heatpipe, Fig. 2(ii) illustrates a conductive heatpipe, and Fig. 4 covers the case of non-zero net mass flux (but no conduction).

As already mentioned the natural state of the geothermal reservoir (insofar as it can be approximated as a one-dimensional steady-state flow) is represented as a path in the flowplane diagram. We refer to this path as a state trajectory. When the permeability is constant k_0 then the state trajectory becomes a segment of the pressure trajectory $k = k_0$, for example the path (ab) in Fig. 2(i) lies along the pressure trajectory $k = 0.3$ md. If there is a slow variation in permeability then the state trajectory will be a curve which lies close to a pressure trajectory. Conversely, if there is a rapid permeability change then the state trajectory lies close to a pressure contour $P = P_0$, for example, a permeability jump from 0.3–0.5 md at a pressure of $P_0 = 100$ bars is represented by the path (bc) in Fig. 2(i). The continuation (cd) represents a further pressure increase at constant permeability (0.5 md). The entire path (abcd) is a state trajectory for the two-phase part of a reservoir containing a single permeability discontinuity.

The saturation (or rather, the relative permeability) at a flowpoint $\mathrm{X}(w, s)$ is determined, as explained above, by drawing the tangent from the point to Γ. If the flowpoint is in the counterflow region Δ (where there are two tangents to Γ) then the tangent on the right must be selected. This ensures that the correct sheet of the flowplane $\mathrm{C}_-: C < 0$ is being used. Variations in saturation along a state trajectory can be easily tracked by this graphical method.

Note that in this study the representation (9) has validity only on the sheet C_- of the flowplane where the saturation wavespeed is negative (points upwards). It is sometimes convenient to analytically extend the pressure trajectories and permeability contours across the boundaries of this region, however it should be remembered that the flowpoints outside C_- have no physical significance (except possible as single-phase transition states, see below). The boundary of C_- is conveniently divided into three parts (see Fig. 1): (a) the liquid boundary $\mathrm{B}_w \equiv \mathrm{B}_w^-$ which is the section $(-\infty < w < 1)$ of the w-axis; (b) the vapour boundary $\mathrm{B}_s \equiv \mathrm{B}_s^-$ which is the section $(-\infty < s < -1)$ of the s-axis; and (c) the stability boundary Γ along which $C = 0$.

3.2. Phase transitions

The geothermal reservoir models discussed in this paper are required to be 'physically realistic', that is, they must be capable of representing the reservoir between the geothermal source and the surface of the earth. Such a model will usually contain one or more single-phase sections bounding the two-phase zone. Young [5] has summarized the selection rules governing phase transitions, and Table 1 from this paper is repeated here for convenience.

The table characterizes the various phase transitions which can occur in one-dimensional hydrothermal flows in terms of saturation changes and the sign of the saturation wavespeed. The symbols are (T) = two-phase, (S) = single-phase vapour, (W) = single-phase liquid, and (TW) means a transition from (T) above to (W) below, etc. The transitional states are restricted to the parts of the flowplane specified in column 5. For each transition there are two possibilities depending on the sign of the wavespeed. Typically, one involves a jump in saturation (a saturation boundary shock), and the other is a smooth transition where the relative permeability $x \equiv k_w$ tends smoothly to its boundary value (0 or 1). Since the BH-BC used in this paper imply $C \leqslant 0$ (pointing upwards) we see from the Table 1 that if single-phase fluid lies over two-phase fluid (ST) or (WT), then there must be a jump transition from the single-phase relative permeability (0 or 1) to some two-phase value which we

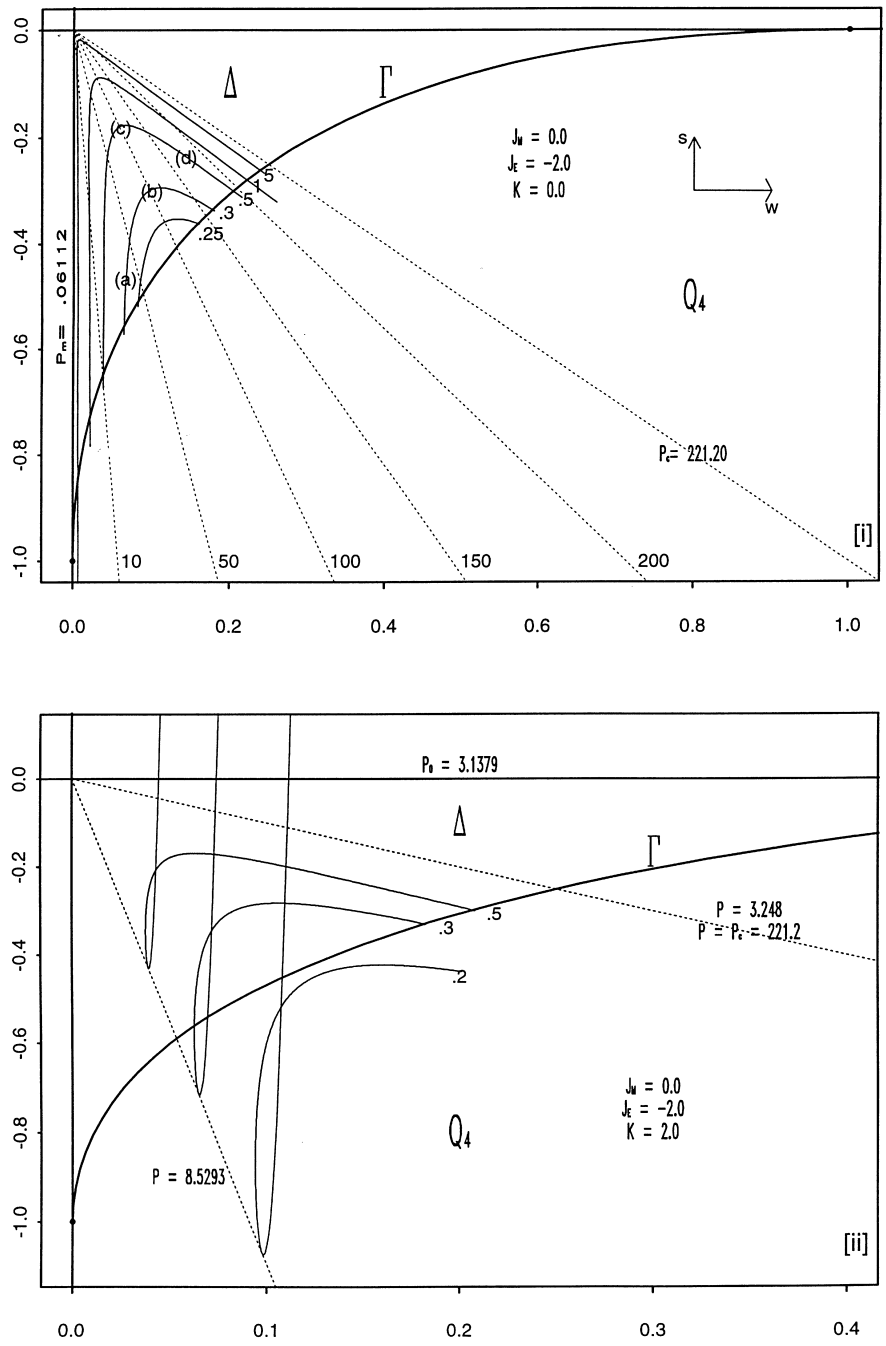

Fig. 2. Flowplane diagram for a geothermal heatpipe. (i) No conduction. The pressure trajectories (solid lines labelled by permeabilities in millidarcies) and contours (dotted lines labelled by pressures in bars) are confined to the fourth quadrant of the flowplane. (ii) With conduction. The pressure trajectories (solid lines labelled by permeabilities in md) have a 'conductive leg' intersecting the w-axis.

have denoted by x_-. Conversely, if two-phase fluid lies over single-phase fluid (TS) or (TW) then there can only be a smooth transition from the appropriate residual saturation to single-phase conditions.

In the flowplane a BH-BC jump transition is represented by a point in the interior of C_-. It is the starting point for the two-phase state trajectory. A smooth transition is represented by a point on the boundary of C_-:

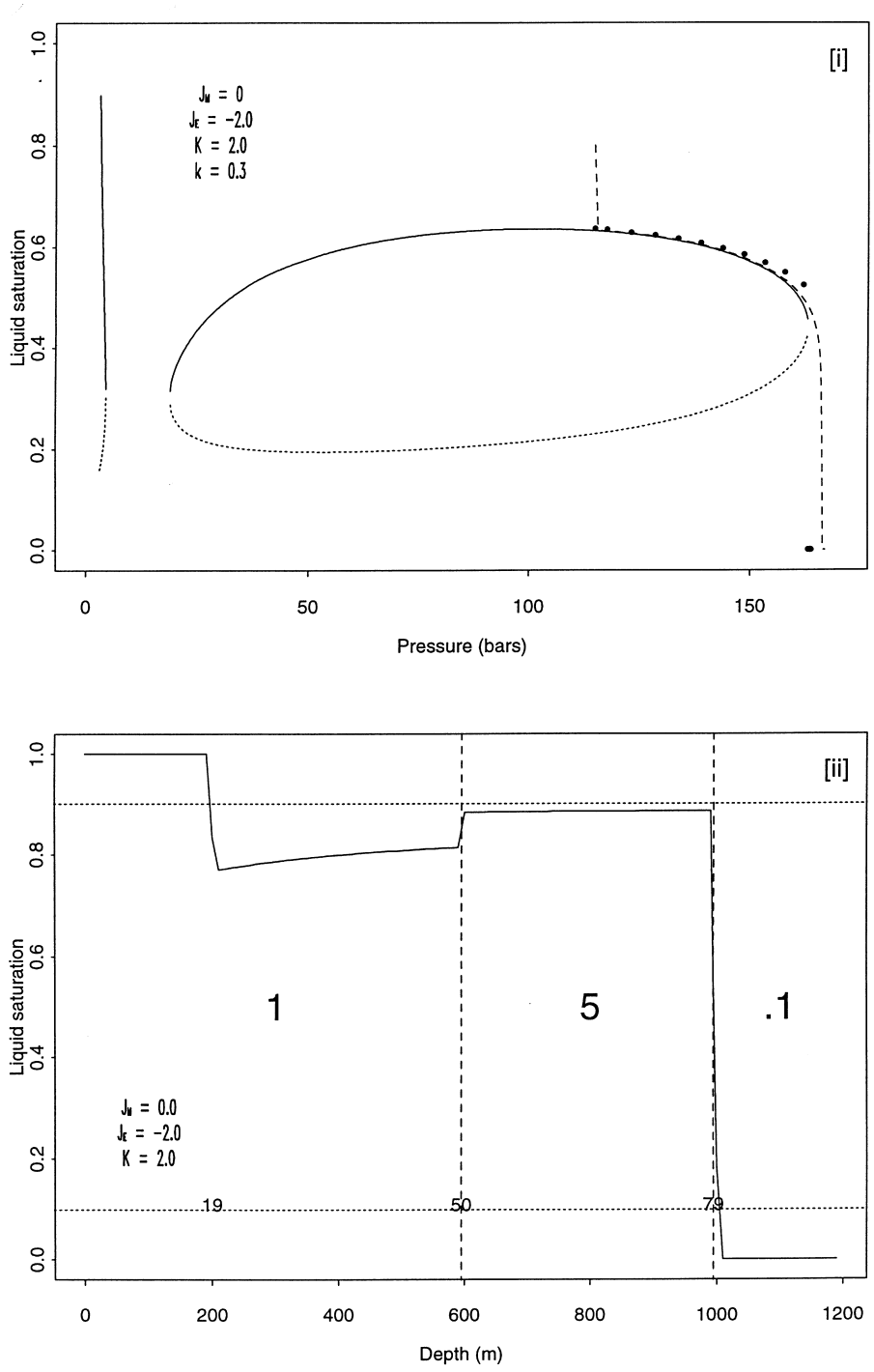

Fig. 3. The geothermal heatpipe. (i) Pressure–saturation diagram. The oval figure formed from the solid and dotted lines is the analytic expression obtained from equations (9) and (11). The section at the left is the low pressure conductive leg. The bullet points are the GTH simulation results for this example. The dashed line is constructed from the TOUGH2 simulation. (ii) Saturation-depth profile for a 1200 m vertical heatpipe (gravity acts to the right) containing two permeability discontinuities denoted by the vertical dotted lines. The permeabilities are given in millidarcies (large bold numbers). Values of mass flux J_M, energy flux J_E, and conductivity K are shown in the figure. The dashed horizontal lines are the residual saturations. Numbers near the bottom of the diagram are the pressures (in bars) at the indicated depths.

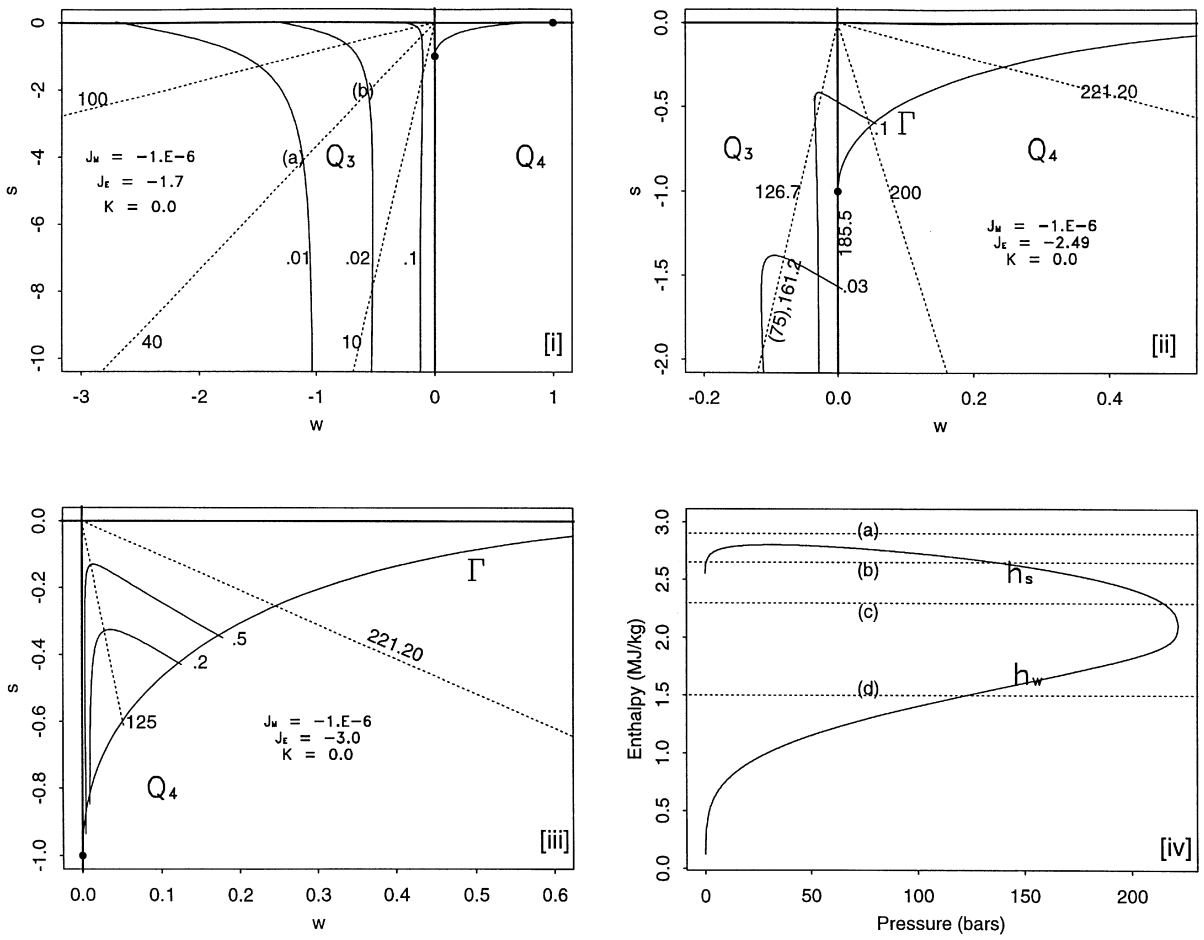

Fig. 4. Flowplane diagrams (i, ii, iii) for three examples of non-conductive steady-state flow. The pressure trajectories are shown as solid lines and are labelled with permeabilities in millidarcies. The radial dotted lines are pressure contours labelled by pressures in bars. Note that some contours have two labels corresponding to the two points of intersection with the pressure trajectory (see diagram (ii)). The fourth diagram (iv) shows vapour and liquid enthalpies in saturated conditions. The four cases in equation (23) are shown (dotted lines).

on B_s for (TS) or on B_w for (TW). It is the end point for two-phase state trajectory, see for example the pressure trajectories in Figs 4[i, ii].

3.3. Terminal state of pressure trajectories which cross Γ

Not all BH-BC state trajectories terminate with a smooth phase transition: Fig. 2(i) shows that all non-conductive heatpipe pressure trajectories intersect the stability boundary Γ. At the point of intersection they possess a definite saturation S_Γ and pressure P_Γ. The same is true for conductive heatpipe, Fig. 2(ii). If there is a net mass throughflow then only some of the trajectories need intersect Γ (Fig. 4).

The question arises as to the terminal state of such trajectories when they are extended as far as, and then beyond, Γ. Consider the alternatives.

(a) The only possible smooth continuation of the trajectory on $C_-: C < 0$ (wavespeed directed upwards) after it intersects Γ is onto the positive sheet of the flowplane $C_+: C > 0$ (wavespeed directed downwards). We show in Appendix A that such a continuation is not possible in the steady-state, and in any case this branch is unstable for the imposed BH-BC.

(b) Secondly, there is the possibility of a jump transition to single-phase conditions. In general a phase transition of this type, (TW) or (TS), is not consistent with the assumed BH-BC, see Table 1. However in the special case when $C = 0$ Table 1 shows that the

Table 1
Permissible phase transitions (selection rules) for hydrothermal flows

Phase transitions	Type	Thermodynamic inequality	Wave speed constraint	Flow plane region	Saturation change
TW	Jump	$s \geqslant 0$	$C \geqslant 0$	Q_1	$x_+ \mapsto 1$
TS	Jump	$w \geqslant 0$	$C \geqslant 0$	C_+	$x_+ \mapsto 0$
WT	Jump	$s \leqslant 0$	$C \leqslant 0$	C_-	$1 \mapsto x_-$
ST	Jump	$w \leqslant 0$	$C \leqslant 0$	Q_3	$0 \mapsto x_-$
TW	Smooth	$s = 0$	$C \leqslant 0$	B_w^-	$1 \mapsto 1$ VR
TS	Smooth	$w = 0$	$C \leqslant 0$	B_s^-	$0 \mapsto 0$ LR
WT	Smooth	$s = 0$	$C \geqslant 0$	B_w^+	$1 \mapsto 1$ VR
ST	Smooth	$w = 0$	$C \geqslant 0$	B_s^+	$0 \mapsto 0$ LR
TT	Jump	$w > 0$, $x < 0$	$C > 0$, $C < 0$	Δ	$x_+ \mapsto x_-$

Notation: VR, vapour residual; LR, liquid residual; values $x_\pm$ are the conjugate saturations (roots of (13)).

jump transition (TS) is formally possible (whereas (TW)—in Q_1—is not).

(c) A third possibility is that a trajectory which includes a point of the neutral stability boundary Γ may not be stable to small perturbations. According to this point of view the jump transition (TS) would not be observed for BH-BC (and steady one-dimensional flow in a homogeneous porous medium), because it would be unstable.

In summary, a steady-state trajectory which intersects the stability boundary is either unstable, or it must terminate in single-phase vapour. The present analysis does not distinguish between these possibilities.

3.4. Permeability discontinuities

In the case of a jump in permeability initiated in the two-phase region, it must be possible to connect the current state k_1 to the new state k_2 by a pressure contour. For a rapid but continuous change in permeability we can imagine that each contour is 'thickened' to a capillary boundary layer within which the 'inner solution' of the capillary flow equations dominates [9]. There are then three possibilities: (a) the new state is two-phase, in this case we have a permeability-induced saturation jump between two two-phase states; (b) the new state is single-phase, either vapour or liquid; or (c) the new state is unstable.

To distinguish between the various possibilities, we first observe that at a phase boundary, the neighbouring single-phase state has a valid representation as a point (w, s) in the flowplane since pressure and temperature still lie on the Clausius–Clapeyron curve. When the permeability is continuous at a phase boundary, Table 1 implies that the single-phase boundary state must lie either (a) in the interior of C_-, which corresponds to a jump transition of type (WT) or (ST), respectively; or (b) on the boundary component $B_s \bigcup B_w$ of C_- which corresponds to a smooth transition of type (TS) or (TW); or (c) on the boundary component Γ of C_-. If, on the other hand, there is a permeability discontinuity then the single-phase boundary state will still be represented by a point in the flowplane, but which may lie outside C_-. The selection rules in Table 1 then require some reinterpretation. We shall explain how to do this in subsequent sections.

4. The geothermal heatpipe

We begin by considering some special classes of diagram, namely those which describe zero net mass flow (with and without conduction). These diagrams are relatively simple; in addition these particular physical mechanisms (conduction, counterflow) have a recognizable geometric signature which can subsequently be identified in the more complicated general class.

The case of zero net mass flow is commonly referred to as a 'heatpipe' in the literature, or sometimes as 'counterflow' (we prefer to reserve the latter term for the more general case when liquid and vapour flows are in opposite directions, but not necessarily of equal magnitude). It is not particularly realistic from the geothermal point of view, although some authors have argued that it provides a satisfactory approximation when the net mass flux is small: White et al. [13] have postulated a heatpipe model for part of the Geysers steam field, and McGuinness [14] has suggested that Larderello in Italy, Matsukawa in Japan and Kawah Kamojang in Indonesia could all be modelled as heatpipes.

McGuinness [9] carries a good summary of recent work. Points at issue are:

(1) Is a heatpipe necessarily vapour-dominated? liquid-dominated? or can it be either? Much of the argument is related to the fact that there can be two solutions for a given steady-state heat flow, one vapour-dominated and one liquid-dominated [9]. Satik et al. [15] analyse the steady-state equations including capillarity, and suggest that only the vapour-dominated solution is obtained in practice. However many experimental results [16–18] suggest the contrary.

(2) What is the influence of applied boundary conditions (top cooling or bottom heating)? McGuinness [9] develops a perturbation expansion of the steady-state capillarity equations, and argues that it is the choice of boundary conditions which determines whether the flow is liquid-dominated or vapour-dominated. In particular, when the system is bottom-heated then the heatpipe will be liquid-dominated, when it is top-cooled the heatpipe will be vapour-dominated. If the 'wrong' solution is selected for the applied boundary conditions in a simulation experiment then the system will quickly become unstable when subject to small perturbations [10, 12]. Young [5] does not include capillarity in the geothermal equations, but uses arguments based on the entropy inequality [19] to arrive at much the same conclusions as McGuinness. However Stubos et al. [4] claim that both vapour- and liquid-dominated solutions are stable, and the solution selection is determined by the past behaviour of the system.

(3) What is the maximum length of a heatpipe? Can it be infinite? Stubos et al. [4] repeat the claim of Udell [18] that a homogeneous heatpipe is of indefinite length unless the heatflow exceeds a certain critical value [equation (14) below], in which case the length is finite. McGuinness [9] argues that it has always a specific finite length. Bau and Torrance [17] reported the appearance of oscillatory instability in their heatpipe laboratory experiments when the length of the two-phase column exceeded a certain fraction of the bed height.

(4) Under what conditions can a multi-layer heatpipe containing phase boundaries evolve? Schubert and Straus [20] postulate a two-layer heatpipe in which a vapour-dominated two-phase layer lies over a quiescent liquid layer. McGuinness [9] and Young [5] are both of the opinion that such a heatpipe would be stable only for TC-BC (top-cooled boundary conditions) which would generally not be appropriate in a geothermal context, however Satik et al. [15] claim that Schubert and Straus' model would be observed for BH-BC. Young [5] presents a general treatment of the stability properties of phase boundaries in the steady state, see Table 1. Stubos et al. [4] give a theoretical description based on capillarity concepts of a bottom-heated liquid-dominated heatpipe model surmounted with a quiescent liquid layer.

(5) Effect of a permeability discontinuity? Stubos et al. state that the model just cited can only terminate (in single-phase vapour at depth) if there is a rapid permeability increase with depth. This is consistent with their contention (mentioned in the Introduction to this paper) that a permeability increase (downwards) in liquid-dominated conditions acts to decrease the liquid saturation.

In the following we will argue for a particular resolution of all these conflicting points-of-view and we will explain how the divergence in opinion has arisen.

4.1. *Zero net mass flow*: *no conduction*

Figure 2(i) shows the pressure trajectories (solid lines) and contours (dotted lines) for the case of zero net mass-flow ($J_M = J_w + J_s = 0$) and zero conduction.

In the heatpipe with zero conduction the energy flux can be written $J_E = (\Delta h)J_s$ and since $J_s < 0$ (vapour travels upwards in a steady-state heatpipe) it follows from equation (9) that the flow states are confined to the quadrant Q_4 of the flowplane, or, more precisely, to the counterflow region $\Delta \subset Q_4$. Note that for a non-trivial heatpipe the pressure trajectories may not intersect either axis, since in that case equation (9) implies $J_E = 0$. A further point is that the zero conduction heatpipe can under no circumstances include a single-phase leg, because in such a region there is no mass flow, and hence no energy flow either.

The character of the pressure trajectories and contours may be deduced from equation (9), or read directly from Fig. 2(i). In the present case the pressure contours are all straight lines emanating from the flowplane origin (as $k \to \infty$). Note that the pressure trajectories must all intersect Γ for some boundary pressure P_Γ less than the critical value, since if $P = P_c$ then $\Delta h = 0 = \Delta\rho$, which here implies $w = \infty$, $s = -\infty$. P_Γ is computed from the expression

$$\omega \equiv \frac{-J_E v_s}{kg\Delta h \Delta\rho} = \frac{v_s}{(\sqrt{v_w} + \sqrt{v_s})^2} \equiv \omega_{\text{crit}} \tag{14}$$

which is obtained by combining equations (9) and (12) (with $J_M = 0 = K$). The quantity ω is termed the dimensionless heat flux, while the right-hand side of equation (14) is commonly referred to as the maximum, or critical, or dry-out heat flux [17, 18, 4]. For two-phase conditions to hold the flow point must lie inside Δ, that is

$$\omega \leqslant \omega_{\text{crit}}. \tag{15}$$

In laboratory experiments both ω and ω_{crit} are usually approximated by constants. It is then often claimed that dry-out to single-phase vapour conditions must occur if the heat throughflow is such that $\omega > \omega_{\text{crit}}$. However in the case of a geothermal heatpipe the pressure dependence of both ω and ω_{crit} must be retained. Then in our interpretation the dimensionless heat flux reaches its dry-out value in every geothermal heatpipe (if sufficiently extended). As shown above a state trajectory cannot be

prolonged beyond this stability boundary: it either becomes unstable or there is a jump transition to single-phase vapour. Since a purely convective heatpipe cannot be connected to a single-phase region, it must therefore become unstable when extended. This conclusion is in contrast to the view of Udell [18] and Stubos et al. [4], that a homogeneous bottom-heated heatpipe (with small enough heat flow) may be extended downwards 'indefinitely'.

In fact Fig. 2(i) shows there may be two pressures which satisfy (14), and P_Γ is the greater of the two. As $-J_E/k$ increases the two pressures approach one another, and eventually become identical, when $\omega J_E(P)/\partial P = 0$. At this point the (analytic continuation of the) pressure trajectory lies entirely below Γ in the region $\bar{\Delta} = Q_4 \backslash \Delta$ and just touches Γ at the double root. For given permeability k this condition defines a maximum heat flux $-J_{E(\max)}(k)$ beyond which no heatpipe is possible, conversely for given J_E it defines a minimum permeability $k_{\min}(J_E)$ such that no heatpipe is possible for $k < k_{\min}$. Figure 2(i) also shows that for large permeabilities the BH-BC heatpipe is liquid-dominated over most of its length. However vapour-dominated conditions can be encountered at the top and bottom of the pipe.

Permeability heterogeneity. If the column contains a permeability contrast then we see from Fig. 2(i) that for Δk positive (for example, from (b)–(c) along the $P = 100$ bar pressure contour) the liquid saturation must increase. This is in the opposite sense to what might be expected from a capillary driven phenomenon. To understand what is involved here we refer to the saturation equation operating in the capillary layer, as given by Stubos et al. [4].

$$\left(-\frac{J'}{\tau}\right)\frac{\partial S}{\partial \xi} + \frac{J}{\tau^2}\frac{\partial \tau}{\partial \xi} = 1 - \left(\frac{w}{k_w} - \frac{s}{k_s}\right). \tag{16}$$

Here τ is a dimensionless permeability, ξ is a dimensionless depth coordinate (positive downwards) and J is Leverett's J-function. The coefficients w, s are identical with the flow coordinates (9) (for this case $J_M = 0 = K$). Let us follow what happens when the dimensionless permeability increases through a strong gradient from an initial value of $\tau = 1$ to a final value $\tau = \tau_1 > 1$. Initially (outside the heterogeneity) the RHS of equation (16) is zero [see (11)]. If the permeability increases this term becomes positive until equilibrium is re-established. Thus inside the layer the saturation gradient is governed by a balance between a positive gravitational contribution (the RHS) and the negative capillary term coupled to the permeability gradient (second term on the left). Initially (just inside the layer) it may often be the case that capillarity dominates and S decreases (the derivative $J' = \partial J/\partial S$ of Leverett's J-function is negative). However eventually the influence of the permeability gradient term will be balanced by the gravitational term and the saturation within the layer will begin to increase. Finally equilibrium is re-established, the LHS of (16) is again zero, and (11) now holds for the new permeability ($\tau = \tau_1$) and the corresponding saturation which can be obtained from this equation (with P constant). The net result (for BH-BC) is a saturation increase as shown by the simulation example Fig. 4. The initial saturation decrease (if it occurs) is hidden within the capillary layer. This is true even in the case of strong permeability gradients as considered by Satik et al. Although a local capillary-driven saturation response to a permeability gradient (permeability increase downwards $\Rightarrow$ liquid saturation decrease) may be observed in laboratory situations, in a geothermal heatpipe only the macroscopic gravitational response (permeability increase downwards $\Rightarrow$ liquid saturation increase) is likely to be noticed.

Let us now apply these ideas to the hypothesis put forward by Straus and Schubert [2], that a permeability contrast is required to explain the existence of vapour-dominated conditions in the natural state of a geothermal reservoir. The obvious corresponding reservoir structure is the boundary between the caprock and the geothermal aquifer. But, according to the argument just presented, this zone of rapidly increasing permeability (downwards) will be associated with a liquid saturation increase, not a decrease. Hence this mechanism as it stands cannot account for the existence of vapour-dominated geothermal reservoirs.

4.2. Zero net mass flow with conduction

In this case the flow coordinate definition (9) simplifies to

$$w = \frac{-v_w}{kg\Delta h\Delta\rho}[J_E + \rho_s g\gamma] \tag{17a}$$

$$s = \frac{v_s}{kg\Delta h\Delta\rho}[J_E + \rho_w g\gamma] \tag{17b}$$

where $\gamma = K\dot{T}_{\text{sat}}$. From equation (17) the flow point $X(w, s)$ is formally located as follows

$$\text{X in second quadrant } Q_2 \Rightarrow -J_E < \rho_s g\gamma \tag{18a}$$

$$\text{X in first quadrant } Q_1 \Rightarrow \rho_s g\gamma < -J_E < \rho_w g\gamma \tag{18b}$$

$$\text{X in fourth quadrant } Q_4 \Rightarrow -J_E > \rho w g\gamma. \tag{18c}$$

Only (18c) is physically acceptable for BH-BC. Thus, the state trajectory is again confined to Δ and the pressures must satisfy the inequality (18c). If J_E has too small a magnitude then there is no BH-BC solution (no negative wavespeed two-phase state): we must have a 'high energy' state satisfying $-J_E > \rho_c g\gamma_c$, or $-J_E/K > 0.0115$ K m^{-1} (see Appendix); if J_E is 'low energy' $-J_E < \rho_c g\gamma_c$ then only positive wavespeed states are possible. Equation (18) also shows that if J_E is high energy then the trajectory will always cross the positive w-axis, but does not intersect the s-axis. The intersection is confined to the physical range $0 < w < 1$ provided $k > k_{\min}$ where

$k_{\min}(J_E, K)$ labels the trajectory passing through the wet point W(1, 0). This minimum permeability value is determined from equation (17) as

$$k_{\min}/K = v_w \dot{T}_{\text{sat}}/\Delta h \tag{19}$$

where the right hand side is evaluated at the pressure $P_0(J_E/K)$ which satisfies $-J_E = \rho_w g \dot{T}_{\text{sat}}$. For the parameter values used in Fig. 2(ii) we find $P_0 = 3.1379$ bars, and $k_{\min}/K = 1.113 \times 10^{-17}$ m^3 K W^{-1}.

Figure 2(ii) shows the pressure trajectories for an example of zero net mass flow with conduction. Pressure contours are again straight lines, but this time can be double-valued (two pressures labelling the same line). Comparing with Fig. 2(i) we see that conduction only affects the low pressure end of the trajectory, adding an additional leg to the pressure locus. The intersection with Γ is defined by an expression similar to equation (14), and this time there can be up to three pressure values which satisfy it. When $k = 0.3$ md the conductive part of the heatpipe is separated from the convective part by Γ. For $k = 0.2$ md the convective leg has disappeared entirely (below Γ) as in the non-conductive case but the conductive leg remains. Further decrease in permeability will move the vertical conductive segment to the right until it intersects the w-axis at $w = 1$. At this point the permeability must have the value $k_{\min}$ given in equation (19). Permeabilities less than this cannot be present in a steady-state conductive heatpipe.

Extended heatpipes. The example shows that the effects noted in the non-conductive heatpipe are present here as well. In particular, a vertically extended heatpipe can only leave the flowplane by crossing Γ. When conduction is present a transition to single-phase vapour is possible at this boundary. Figure 3(i) shows a simulation example illustrating this. The bullet points are the GTH (Georgia Tech Hydrothermal) simulation results obtained by Wenyue Xu (School of Earth and Atmospheric Sciences, Georgia Institute of Technology, Atlanta, GA : private communication) using 12 grid blocks each 100 m deep, and two small 0.01 m boundary blocks with the upper boundary held at $P = 115$ bars, $S = 0.6359$ and $J_M = 0$, $J_E = -2$ W m^{-2} at the lower boundary. The simulation data lies close to the $C < 0$ branch of the analytic curve, and a stable transition (TS) is obtained near $C = 0$.

This numerical solution was checked with the TOUGH2 simulator [21] using a total of 115×10 m gridblocks, and a similar results was obtained. The small divergence in the numerical treatments can be attributed to alternative choices of the thermodynamical functions. Note that since $C < 0$ the upper saturation boundary condition should be irrelevant. This is shown to be the case in the TOUGH2 simulation results, where the boundary saturation is held at $S = 0.8$, but is present only as a boundary discontinuity.

A further point is that the TOUGH2 curve is actually a double line, the two cases being identical except for the respective presence or absence of capillarity (using the Leverett J-function). Although physical capillarity is evidently insignificant in the simulation, numerical upstreaming apparently assumes an equivalent role especially near $C = 0$ where convective effects disappear [10]. Upstreaming presumably accounts for the divergence of the TOUGH2 numerical solution from the theoretical curve in Fig. 3(i).

The zero point itself is only neutrally stable, and passage through it is a delicate matter. Near $C = 0$ numerical stability is highly dependent on the selection of the initial conditions. If these are chosen too far from the final steady state then numerical instabilities appear. These are usually cyclical in nature with a typical period of 10 000 years. The oscillations can be mild (temperature fluctuations of a few degrees at depth) or they may involve a periodic phase change (two-phase/single-phase vapour).

Multilayer sequences. If conduction is present then the two-phase part of the heatpipe may be surmounted by a single-phase column of immobile fluid. Referring to Table 1 we see that this must be liquid (WT) (the alternative (ST) is excluded since the trajectories must be contained in $\Delta \subset Q_4$).

Permeability heterogeneity. The conductive heatpipe shows a similar behaviour to the non-conductive one with respect to permeability contrasts. In particular for BH-BC a permeability increase (downwards) induces a corresponding increase in the liquid saturation. However with conduction there is the additional possibility that the two-phase state may be terminated by a permeability discontinuity. From Fig. 2(ii) we see that in this case the single-phase boundary state must lie in $\bar{\Delta} = Q_4 \backslash \Delta$ where $w > 0$. Hence from Table 1 the transition must be (TS). Although such a trajectory crosses the stability boundary Γ it does so within the capillary boundary layer with which each pressure contour is surrounded. The stability argument no longer applies when capillarity is dominant.

In summary, possible multilayer sequences for a conductive geothermal (bottom-heated) heatpipe are as follows :

(1) For a homogeneous medium : stationary single-phase liquid–liquid-dominated two-phase–stability boundary–stationary single-phase vapour (W-T_W-Γ-S) ;
(2) For a homogeneous medium : stationary single-phase liquid–liquid-dominated two-phase → unstable when extended (W-T_W → U) ;
(3) In the presence of a negative permeability discontinuity (permeability decrease) : stationary single-phase liquid–liquid-dominated two-phase–[discontinuity]–stationary single-phase vapour (W-T_W-[D]-S).

We illustrate these points with some results from a simulation of one-dimensional flow. Figure 3(ii) shows the saturation profile for a heatpipe containing two permeability discontinuities. In the figure gravity acts to the

right and the horizontal dotted lines are the residual saturations. There is zero net mass throughflow, the energy flow is $J_E = -2.0$ W m^{-2} and conductivity is $K = 2$ W m^{-1} K^{-1}. The upper surface boundary condition is $P_0 = 10^5$ Pa and $T_0 = 15$°C.

Figure 3(ii) is based on numerical results using the TOUGH2 geothermal simulator [21]. A vertical section of depth 1200 m within a geothermal reservoir has been approximated as a one-dimensional column. Starting from an initial single-phase state of constant pressure and temperature the boundary conditions are applied at top ($P = P_0, T = T_0$) and bottom (J_M, J_E), and the system is run to steady-state. In this case a phase boundary appears, separating an upper quiescent single-phase liquid zone from an underlying two-phase region. The location of this interface is determined by the upper boundary condition [6] and the permeability distribution; note that it is generally not coincident with the permeability discontinuity. The saturation jump at the interface consists of two parts: a jump through the immobile steam saturations which are always excluded in the steady-state [22]; and an additional jump to a saturation for which both phases are mobile. Piecewise linear relative permeability functions have been employed in the simulation with $S_{rw} = 0.1 = S_{rs}$; but note that all the results in this paper are independent of the choice of relative permeability function satisfying the normality condition (1). As a partical check on some results the simulations have been run both with capillarity (using Leverett's J-function) and without. The results are essentially identical. This confirms that our formulation of the steady-state problem represents the macroscopic effects of capillarity correctly.

Below the phase boundary (in this example at about 19 bars) there is counterflow within the heatpipe. The liquid saturation then increases until the first permeability discontinuity (a permeability increase from 1–5 md) is encountered at 595 m (about 50 bars). This induces a step increase in liquid saturation. After this there is a further slow increase in saturation. Thus far the profile is qualitatively similar to the state trajectory (abcd) shown in Fig. 2(i) (although the leg (cd) as selected—for reasons of clarity—actually involves a saturation decrease).

The second permeability discontinuity (a permeability decrease from 5–0.1 md) occurs at 995 m (about 79 bars). Referring to Fig. 2(ii) we see that the step decrease is of sufficient magnitude to take the flowstate across the stability boundary Γ into the single-phase part of the flowplane $\bar{\Delta}$. We have argued that this state must be single-phase vapour, and the simulated saturation profile in Fig. 3(ii) confirms this.

Summary. Let us summarize our results in terms of the issues raised at the beginning of this section. Implicit in our argument is the idea that the steady-state boundary conditions determine the sign of the saturation wavespeed, which implies the selection of a particular saturation branch for the heatpipe. For BH-BC the heatpipe is always liquid-dominated. Experimental evidence [16–18] supports this contention. The vapour-dominated heatpipe of Schubert and Straus [20] is unstable unless the boundary conditions are reversed, that is, pressure and temperature are fixed at depth and heat is extracted at a fixed rate from the surface. The liquid-dominated two-phase heatpipe can be connected to an overlying quiescent single-phase liquid layer, but if extended vertically downwards it either loses stability, or possibly connects to single-phase vapour with a jump across the stability boundary. A negative permeability contrast (permeability decreases downwards) induces a liquid saturation decrease, and if the discontinuity is of sufficient magnitude then the heatpipe may terminate in single-phase vapour. Our evidence is presented in Figs 2(i) and (ii), and in the simulation example (Fig. 3(ii)). This is consistent with the rule for the termination of the heatpipe just given. The opposite effect noted by Stubos et al. [4] (permeability decrease → saturation increase) occurs only inside the capillary layer and has no influence outside it.

Conversely, a positive permeability contrast will induce a saturation increase (wetter conditions). The statement by Stubos et al. [4], that a bottom-heated heatpipe may only terminate (in single-phase vapour) if there is a substantial increase in permeability (with increasing depth) somewhere in the medium, refers to a capillary-mediated effect which can be deduced from equation (16), see Stubos et al. for details. We have never observed this effect in our simulations. It seem likely that for capillary dry-out the permeability increase must occur over a small fraction of the capillary layer. The other possibilities detailed here for heatpipe termination, namely: termination in single-phase vapour in response to a permeability decrease, or progression to single-phase vapour through the stability boundary in a homogeneous medium, do not appear to have been explicitly noted by Stubos et al. [4].

Furthermore, we do not believe that a heatpipe may be 'infinitely long for low heat flux' [18]. On the contrary, numerical simulations show that an extended heatpipe often becomes unstable when continued past the stability boundary Γ. The oscillations reported by Bau and Torrance [17] may be experimental evidence of the instability. We suspect that overlooked or unreported instabilities may have occurred in other laboratory heatpipe experiments.

The argument for an infinitely long heatpipe appears to result from ignoring the pressure dependence of the thermodynamical quantities in the steady-state equations [9]. This might seem justified in a laboratory heatpipe experiment where pressures are more or less constant, but it leads to the wrong conclusions when extrapolated to the scale of a geothermal heatpipe (several kilometres).

In our opinion there has been some confusion between the inner and outer levels of the solution [9]. The constant pressure assumption is essentially a boundary layer approximation and leads to error if applied to portions of the heatpipe outside the boundary layer.

5. Non-zero net mass flow: no conduction

Next we consider the case of non-zero net mass flow when conduction is zero, or can be ignored. Again this is not very realistic for a geothermal reservoir, but it provides an interesting comparison with the general case when conduction is not negligible. The flow coordinate transformations are now

$$w = \frac{-v_w}{kg\Delta h\Delta\rho}[J_E - h_s J_M] = \frac{v_w J_w}{kg\Delta\rho} \tag{20a}$$

$$s = \frac{v_s}{kg\Delta h\Delta\rho}[J_E - h_w J_M] = \frac{v_s J_s}{kg\Delta\rho} \tag{20b}$$

where J_w, J_s are the flows of liquid and vapour, respectively. From (20) we derive the analogue of (18) for the flowpoint $X(w, s)$ in terms of $h \equiv J_E/J_M$, the flowing enthalpy (a constant):

X in fourth quadrant $Q_4 \Rightarrow h > h_s$ (21a)

X in third quadrant $Q_3 \Rightarrow h_w < h < h_s$ (21b)

X in first quadrant $Q_1 \Rightarrow h_w < h < h_s$ (21c)

X in second quadrant $Q_2 \Rightarrow h < h_w$. (21d)

For BH-BC only (21a) and (21b) are acceptable. The trajectories may cross either axis in the range $-\infty < w$, $s < 0$. Intersection occurs when

$$h_s(P) = h \Leftrightarrow w = 0, s = v_s J_M/kg\Delta\rho \tag{22a}$$

$$h_w(P) = h \Leftrightarrow s = 0, w = v_w J_M/kg\Delta\rho. \tag{22b}$$

Further detail may be derived from the two-phase enthalpy/pressure diagram Fig. 4(iv): from this diagram and equation (22) we deduce the following physical configurations

low $0 < h < h_c$ 1 intersection on w-axis, confined to Q_3 (23a)

intermediate $h_c < h < h_{sM}$ 1 or 2 intersections on s-axis (23b)

high $h > h_{sM}$ confined to Q_4 (23c)

where h_{sM} is the maximum enthalpy of vapour in saturated conditions and h_c is the enthalpy at the critical point. The Appendix lists the numerical values of these quantities.

Figures 4(i)–(iii), show some representative examples of Cases (23a)–(23c) respectively. It is not necessary to comment on these diagrams in detail, but we shall emphasize the following points:

(1) The phase selection rules given Table 1 do not apply to the zero conduction example, but it is easy to see that in this case the state trajectory can only terminate in single-phase liquid. However our main interest is in the geometrical characteristics of the flowplane trajectories. Therefore we shall not consider multi-layer models further in this section.

(2) In the low enthalpy class (23a) both phases flow upwards and the trajectory is confined to Q_3, see Fig. 4(i). For high enthalpy (23c) the two-phase state is confined to Δ as in Fig. 4(iii), the vapour phase flows up, the liquid down (counterflow), and the trajectories are similar to those in Fig. 2(i) (zero net mass flow with zero conduction).
If $h_c < h < h_{sM}$ [intermediate enthalpy, class (23b)] then the trajectories may be confined entirely to Q_3 (concurrent flow), or they may contain an upper leg where flow is concurrent, and a lower leg where there is counterflow. To distinguish between these possibilities we level the trajectory which passes through the dry point S(0, −1) by k_d then if $k > k_d$ at depth the pressure trajectory will ultimately intersect Γ, but if $k < k_d$ then the trajectory will intersect the vapour boundary B_s. The drypoint permeability $k_d(J_E, J_M)$ is determined from equation (20) with $w = 0, s = 1$, that is,

$$h_s(P) = h, \quad k = \frac{-v_s J_M}{g\Delta\rho} \tag{24}$$

which has a solution for $h_c < h < h_{sM}$ (if $h > h_{sM}$ then the trajectory is confined to Q_4). Here the first equation determines the drypoint pressure $P = P_d$ which is then substituted into the second equation to fix $k = k_d$. If there are two values of P_d then the greater must be taken.

(3) The pressure contours are again straight lines (s/w = const) emanating from the origin. This has an important consequence, namely that a step increase in permeability (for example, from (a) to (b) in Fig. 4(i)) is always associated with an increase in liquid saturation. Since a gradual increase can be constructed from small steps, the general conclusion is that a positive permeability contrast (permeability increase with depth) acts to increase liquid content. This is in agreement with the intuitive notion that a permeability increase should produce a wetter environment.

6. Summary

In Part I of this paper we have given a general introduction to the flowplane method, and shown how it may be used to represent—as a state trajectory in the flowplane diagram—the steady-state of a one-dimensional two-phase geothermal reservoir. Pressure trajectories define the vertical pressure profile of a homogeneous

reservoir, pressure contours track the flow across a permeability discontinuity. The flowplane method ignores the inner structure of the capillary boundary layers, but, when correctly interpreted, it provides selection rules which specify uniquely the (stable) state trajectory relative to the given boundary conditions. In the case of geothermal boundary conditions (BH-BC) the trajectory is selected by the requirement that the saturation wavespeed be negative (upwards-pointing).

The classification of geothermal flows using the flowplane method begins in Part I by considering the geometrical character of the pressure trajectories and contours of some simple examples. In the case of a heatpipe without conduction the state trajectories are confined to the fourth quadrant of the flowplane, and may not intersect the flow axes. When conduction is added a characteristic 'conductive leg' is appended to the pressure trajectories. In the case of non-zero net mass flow, but with no conduction, there is a natural division into high, intermediate, and low enthalpy flows. The pressure trajectories belonging to the low enthalpy flows are all confined to the third quadrant of the flowplane (concurrent flow), and exit through the liquid boundary segment B_w. The high enthalpy flows are confined to the counterflow region Δ of Q_4. Intermediate flows have pressure trajectories of two types: for low permeabilities the trajectories lie entirely in Q_3 and exit the flowplane through the vapour boundary B_s; for high permeabilities they begin with concurrent flow in Q_3, then cross into the counterflow region Δ, and exit through the stability boundary Γ.

We used the flowplane diagram to determine the character of the bottom-heated geothermal heatpipe, and compared our results with those of other authors. In particular, we showed that the two-phase part of the heatpipe could be surmounted with a quiescent liquid layer, and that oscillatory instability often sets in when the heatpipe is extended vertically downwards. Transition to single-phase vapour through the stability boundary was possible provided the initial conditions were close to the final state. Both the unstable and stable heatpipes could be used as idealized natural state reservoir models, but note that vapour-dominated conditions are only encountered—if at all—at considerable depth. The heatpipe could also be terminated (in single-phase vapour) at any depth by a negative permeability discontinuity (rapid permeability decrease).

The pressure contours in all the special cases considered in Part I were radial straight lines emanating from the flowplane origin ($s/w = \text{const}$), which implies that a permeability increase (downwards) always acts to increase the liquid saturation. This is not in conformity with the hypothesis that the positive permeability gradient between the caprock and the underlying geothermal aquifer can act to induce vapour-dominated conditions in the latter [2, 3]. Thus some other factor must be sought to account for the existence of vapour-dominated geothermal reservoirs. This will be described in Part II of this paper.

Acknowledgments

Extensive discussion with Yanis Yortsos (Department of Chemical Engineering, University of Southern California) has clarified the connection between the capillary mechanism and the entropy inequality. Thanks to Wenyue Xu (School of Earth and Atmospheric Sciences, Georgia Institute of Technology) who has provided the simulation data for the $C = 0$ transition shown in Fig. 3(i).

Appendix

Thermodynamic properties. The thermodynamic properties used in the computations are, with one exception, those listed in [23]. The exception is the kinematic viscosity which is taken from [24].

Some useful saturated values are:

The minimum temperature two-phase state is given in the steam tables as $T_m = 0.01°\text{C}$. At this temperature $P_m = 6112$ Pa, and $h_{wm} \equiv 0.0$, $h_{sm} = 2.5016$ MJ kg^{-1}, $\rho_{sm} = 4.85053 \times 10^{-3}$ kg m^{-3}, $\rho_{wm} = 999.7765$ kg m^{-3}, $v_{wm} = 1.7918 \times 10^{-6}\,\text{m}^2\,\text{s}^{-1}$, $v_{sm} = 1899.975 \times 10^{-6}\,\text{m}^2\,\text{s}^{-1}$, $\acute{T}_{\text{sat}}(P_m) = 0.0225\ \text{Pa}^{-1}\,\text{K}$.

The maximum enthalpy of saturated steam is $h_{sM} = 2.8023$ MJ kg^{-1} at a temperature of about $T = 235°\text{C}$ ($P = 30.632$ bars).

The critical point is at $T = T_c = 374.15°\text{C}$ ($P = P_c = 221.20$ bars). At the critical point the distinction between vapour and liquid disappears. Thus, at this point we have $h_w = h_s = h_c = 2.1074$ MJ kg^{-1}, $v_w = v_s = v_c = 0.1218 \times 10^{-6}$ m^2 s^{-1}, $\rho_w = \rho_s = \rho_c = 314.73$ kg m^{-3}. Also we find that the saturation temperature derivative at the critical point is $\acute{T}_{\text{sat}}(P_c) = 3.7100 \times 10^{-6}\ \text{Pa}^{-1}\,\text{K}$.

The behaviour of the saturated liquid and vapour enthalpies over the temperature range $T_m < T < T_c$ is illustrated in Fig. 4(iv).

Flowplane boundary Γ. Here we shall demonstrate that a smooth transition from one flowplane sheet to the other is not possible in the steady-state. We use the saturation equation (10) specialized to the steady-state

$$C(S, P, P_z)\frac{\partial S}{\partial z} = \delta(S, P, P_z). \tag{25}$$

We can use the relations $J_M = J_M(S, P, P_z)$, $J_E = J_E(S, P, P_z)$ to eliminate P_z from (25), and to express P as a single-valued function of S, J_M and J_E. Near Γ: $C = 0$ the functions C and δ may be written

$C = -(S-S_\Gamma)a_1(J_M, J_E)+\cdots$ and $\delta = \delta_0(J_M, J_E)+\cdots$ where S_Γ is the value of S on Γ. It may be shown that a_1 and δ_0 are both positive. Then (25) integrates to

$$(S-S_\Gamma)^2 = -\frac{2\delta_0}{a_1}(z-z_\Gamma)+\cdots \quad (26)$$

where z_Γ is the value of z on Γ. Equation (26) can only be satisfied for real S if $z \leqslant z_\Gamma$. This remains true for both the negative sheet $C < 0$, $S > S_\Gamma$ and the positive sheet $C > 0$, $S < S_\Gamma$. Thus, in no case can the trajectory be extended (smoothly) through Γ: $C = 0$.

References

[1] Schubert G, Straus JM. Gravitational stability of water over steam in vapor-dominated geothermal systems. J Geophys Res 1980;85:6505–12.

[2] Straus JM, Schubert G. One-dimensional model of vapor-dominated geothermal systems. J Geophys Res 1981;86(B10):9433–8.

[3] Ingebritsen SE, Sorey ML. Vapor-dominated zones within hydrothermal systems: evolution and natural state. J Geophys Res 1988;93(B11):13 365–55.

[4] Stubos AK, Satik C, Yortsos YC. Effects of heterogeneity on vapor–liquid counterflow in porous media. Int J Heat Mass Transfer 1993;36(4):967–76.

[5] Young, RM. Phase transitions in one-dimensional steady-state hydrothermal flows. J Geophys Res 1996;101(B8):18 011–22.

[6] Sheu JP, Torrance KE, Turcotte DL. An experimental study of two-phase convection in a porous medium with applications to geological problems. J Geophys Res 1977;82:2045–53.

[7] Grant MA, Donaldson IG, Bixley PF. Geothermal Reservoir Engineering. New York: Academic Press, 1982. p. 317.

[8] Piquemal J. Saturated steam relative permeabilities of unconsolidated porous media. Transport in Porous Media 1994;17:105–20.

[9] McGuinness MJ. Steady solution selection and existence in geothermal heat pipes—I. The convective case. Int J Heat Mass Transfer 1996;39:259–74.

[10] McGuinness MJ, Blakeley M, Pruess K, O'Sullivan MJ. Geothermal heat pipe stability: solution selection by upstreaming and boundary conditions. Transport in Porous media 1993;11:71–100.

[11] Kissling W, McGuinness M, Weir G, White S, Young R. Vertical two-phase flow in porous media. Transport in Porous Media 1992;8:99–131.

[12] Young RM. Two-phase geothermal flows with conduction and the connection with Buckley–Leverett theory. Transport in Porous Media 1993;12:261–78.

[13] White DE, Muffler JP, Truesdell AH. Vapor-dominated hydrothermal systems compared with hot-water systems. Econ Geology 1971;66:75–97.

[14] McGuinness MJ. Geothermal heatpipes—just how long can they be? Proc 15th N.Z. Geothermal Workshop. Auckland University, 1993. pp. 259–66.

[15] Satik C, Parlar M, Yortsos YC. A study of steady-state steam–water counterflow in porous media. Int J Heat Mass Transfer 1991;34(7):1755–72.

[16] Cornwell K, Nari BG, Patten TD. Observation of boiling in porous media. Int J Heat Mass Transfer 1976;19:236–8.

[17] Bau HH, Torrance KE. Boiling in low-permeability porous materials. Int J Heat Mass Transfer 1982;25(1):45–55.

[18] Udell KS. Heat transfer in porous media considering phase change and capillarity—the heat pipe effect. Int J Heat Mass Transfer 1985;28(2):485–95.

[19] Whitham GB. Linear and Nonlinear Waves. New York: Wiley, 1974.

[20] Schubert G, Straus JM. Steam–water counterflow in porous media. J Geophys Res 1979;84:1621–8.

[21] Pruess K, TOUGH2—a general-purpose numerical simulator for multiphase fluid and heat flow. LBL-29400, May, 1991.

[22] Reda DC, Eaton RR. Influence of steam/water relative permeability models on predicted geothermal reservoir performance: a sensitivity study. Paper presented to the Sixth Annual Workshop on Geothermal Reservoir Engineering. Stanford University, 16–18 December 1980.

[23] United Kingdom Committee on the Properties of Steam. UK Steam Tables in SI Units 1970. London: Edward Arnold Ltd, 1970.

[24] Schmidt E. In: Ulrich Grigull, editor. Properties of Water and Steam in SI-Units. Springer-Verlag, 1979. p. 190.